Kinetic and Thermodynamic Investigations of the Photochromism and Solvatochromism of Semipermanent Merocyanines

A. V. Metelitsa,[†] J. C. Micheau,[‡] N. A. Voloshin,[†] E. N. Voloshina,[†] and V. I. Minkin[†]

Institute of Physical Organic Chemistry, Stachka Str., 194/2, Rostov on Don 344090, Russia, and IMRCP, UMR au CNRS no. 5623, Université Paul Sabatier, F-31062 Toulouse, France

Received: February 2, 2001; In Final Form: May 2, 2001

The photochromic and solvatochromic behavior of four phenanthroline-containing spirooxazines bearing various alkyl long-chain substituents has been investigated in different polar and nonpolar solvents at various temperatures. These derivatives always appeared in an equilibrium mixture of spiro forms and open merocyanines. Depending on the substituents and the solvents, the percentage of the spontaneous merocyanine open form ranged from less than 10% to more than 30%. These results have been corroborated by independent NMR and photokinetic analysis. The main spectroscopic, thermodynamic, and photochromic parameters of such photo- and solvatochromic systems have been determined. Special illustrative diagrams showing quantitative substituent and solvent effects on absorption wavelengths, molar absorption coefficients, thermal equilibrium, interconversion rate constant, and quantum yields have been established. The two *O*-alkyl long-chain-substituted compounds **3** and **4** behave similarly, as do the *N*-alkyl derivatives **1** and **2**. Opposition between polar and nonpolar solvents was also clearly illustrated. A global energy diagram including a short-lived cisoid merocyanine intermediate allows the interpretation of all solvent and temperature effects in terms of the relative solvation of the various short- and long-lived species and transition states.

Introduction

Photochromes are those substances that undergo reversible molecular rearrangements between two states characterized by different spectral parameters. Such properties are of interest to provide systems that could operate as molecular electronic switches or as new elements for optochemical memories. Photochromic compounds applicable to such devices should possess a large variety of properties, including high thermal stability, high photoreaction quantum yields, feasability of biphotonic photochromism, and insensitivity to photodegradation. However, molecules combining all these requirements have yet to be synthesized.[1]

Among the numerous organic photochromic substances available, it is possible to identify classes exhibiting some of the required parameters. A careful examination of their basic properties is needed in each particular case. Our purpose is to quantitatively determine the photochromic parameters including environmental factors such as solvent effects and temperature. From this point of view, phenanthroline-containing long-chain spirooxazines[2] are of interest. They are expected to have a greater photostability than the more widely studied structurally similar spiropyrans. Moreover, the presence of both a hydrophobic long chain and a polar phenanthroline moiety gives to the molecule an amphiphilic character. This is a decisive advantage for probing the microenvironment and polarity changes that occur during the photoisomerization process. In the simplest case (i.e. without taking into account the distribution of the short-lived merocyanines isomers[3]), the photochromism of spirooxazines is related to the presence of two isomers: the spiro UV-absorbing closed form (**A**) and the most stable open merocyanine TTC form (**B**), where ring opening allows a larger conjugation and consequently gives visible absorption.[4]

The photochromic effect can be interpreted by the photoisomerization of **A** to **B** (I) and the thermal reversion[5] of **B** to **A** (II). However, more complicated behavior is also found, namely the superimposition of photobleaching of **B** to **A** (III) and the thermal coloration of **A** to **B** (IV). The presence of the thermal equilibrium (II + IV) (**B** → **A**; **A** → **B**) makes the system spontaneously colored, and hence, the merocyanine open form **B** is semipermanent. In such a case, the most parcimonious mechanism that can be postulated is a two-species, four-process scheme:

$$\mathbf{A} \rightarrow \mathbf{B}\ (h\nu;\ \Phi_{AB}) \qquad \text{(I)}$$

$$\mathbf{B} \rightarrow \mathbf{A}\ (\Delta;\ \mathbf{k}_{BA}) \qquad \text{(II)}$$

$$\mathbf{B} \rightarrow \mathbf{A}\ (h\nu;\ \Phi_{BA}) \qquad \text{(III)}$$

$$\mathbf{A} \rightarrow \mathbf{B}\ (\Delta;\ k_{AB}) \qquad \text{(IV)}$$

Such photochromic systems are likely to be common but are often difficult to investigate. For instance, it could be necessary to increase the temperature to observe the **A** → **B** thermoprocess (IV) or to use special equipment to record the weak **B** → **A** photoprocess (III). This is the probable reason such systems have been described in a simpler way, i.e. taking into account only two or three processes instead of four.[6] There are several examples in the literature of quantitative descriptions of two-process (I + II[7] and II + IV[8]) or three-process (I + II + III[9] and I + II + IV[10]) photo- or thermochromic systems. However, quantitative analysis of complete four-process systems remains to be achieved.

In this paper, we propose to quantitatively investigate the first experimental example of a I + II + III + IV four-process system

[†] Institute of Physical Organic Chemistry.
[‡] Université Paul Sabatier.

10.1021/jp010419r CCC: $20.00
Published on Web 08/25/2001

SCHEME 1

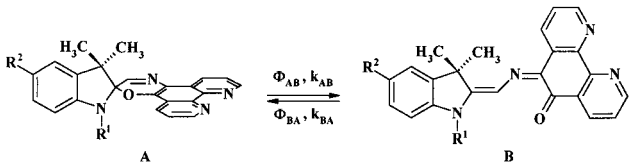

in the spirooxazine series. We describe several cases in which, under normal conditions, it was possible to simultaneously observe thermal and photochemical equilibria between the two forms. Although the problem would be made easier if one or two isomers could be separated for quantitative spectral determination,[11] no isolation was possible in these cases due to the presence of the thermal equilibrium. The only way to determine all the photochromic and spectral parameters was to use photokinetic analysis[12] of the absorbance vs time kinetic curves recorded under continuous monochromatic irradiation at several independent wavelengths. The direct and reverse quantum yields of photocoloration and photobleaching and the spectral, kinetic, and thermodynamic parameters were obtained for the differently substituted long-chain spirooxazines in several solvents.

Experimental Part

The following compounds were studied in various spectroscopic grade solvents: acetonitrile (A), ethanol (E), methanol (M), toluene (T), and in some cases *n*-heptane (H). For the structures of the spirooxazines, please refer to the general formula shown in Scheme 1. The substituents are as follows:

	1	**2**	**3**	**4**
R1	CH_3	*n*-$C_{16}H_{33}$	CH_3	CH_3
R2	H	H	*n*-OC_9H_{19}	*n*-$OC_{16}H_{33}$

(a) Synthesis. Compounds **1** and **4** were prepared according to a previously described method.[13] Compounds **2** and **3** were obtained by coupling 6-hydroxy-5-nitroso-1,10-phenanthroline with substituted 2,3,3-trimethyl-3*H*-indolium iodides according to the method described for the synthesis of compounds **1** and **4**.

3,3-Dimethyl-1-hexadecylspiro[indoline-2,2′-[2H]bipyrido-[3,2-f][2,3-h][1,4]benzoxazine] (***2***). Yield: 45%. Mp: 91−92 °C. Anal. Calcd for $C_{39}H_{50}N_4O$: C, 79.28; H, 8.53; N, 9.48. Found: C, 79.33; H, 8.56; N, 9.40. ^{1}H NMR ($CDCl_3$): δ 0.85 (3H, t, J = 6.9 Hz, 1-$C_{16}H_{33}$), 1.21 (26H, m, 1-$C_{16}H_{33}$), 1.34 (3H, s, 3-CH_3), 1.38 (3H, s, 3-CH_3), 1.61 (2H, m, 1-$C_{16}H_{33}$), 3.19 (2H, m, 1-$C_{16}H_{33}$), 6.60 (1H, d, J = 7.8 Hz, 7-H), 6.89 (1H, td, J = 7.5 Hz and 0.9, 5-H), 7.09 (1H, dd, J = 7.4 and 1.2 Hz, 4-H), 7.21 (1H, td, J = 7.7 and 1.3 Hz, 6-H), 7.52 (1H, dd, J = 8.3 and 4.4 Hz, 6′-H), 7.67 (1H, dd, J = 8.4 and 4.3 Hz, 11′-H), 7.81 (1H, s, 3′-H), 8.42 (1H, dd, J = 8.3 and 1.8 Hz, 12′-H), 8.94 (1H, dd, J = 8.3 and 1.7 Hz, 5′-H), 9.07 (1H, dd, J = 4.3 and 1.7 Hz, 10′-H), 9.13 (1H, dd, J = 4.4 and 1.8 Hz, 7′-H).

5-Nonyloxy-1,3,3-trimethylspiro[indoline-2,2′-[2H]bipyrido-[3,2-f][2,3-h][1,4]benzoxazine] (***3***). Yield: 52%. Mp: 110−111 °C. Anal. Calcd for $C_{33}H_{38}N_4O_2$: C, 75.83; H, 7.33; N, 10.72. Found: C, 75.77; H, 7.36; N, 10.78. ^{1}H NMR ($CDCl_3$): δ 0.87 (3H, t, J = 6.9 Hz, 5-OC_9H_{19}), 1.27 (10H, m, 5-OC_9H_{19}), 1.34 (3H, s, 3-CH_3), 1.39 (3H, s, 3-CH_3), 1.45 (2H, m, 5-OC_9H_{19}), 1.77 (2H, m, 5-OC_9H_{19}), 2.69 (3H, s, 1-CH_3), 3.93 (2H, t, J = 6.6 Hz, 5-OC_9H_{19}), 6.47 (1H, d, J = 9.1 Hz, 7-H), 6.74 (2H, m, 4-H, 6-H), 7.52 (1H, dd, J = 8.3 and 4.4 Hz, 6′-H), 7.66 (1H, dd, J = 8.4 and 4.3 Hz, 11′-H), 7.82 (1H, s, 3′-H), 8.40 (1H, dd, J = 8.3 and 1.8 Hz, 12′-H), 8.95 (1H, dd, J = 8.3 and 1.8 Hz, 5′-H), 9.05 (1H, dd, J = 4.3 and 1.8 Hz, 10′-H), 9.12 (1H, dd, J = 4.4 and 1.8 Hz, 7′-H).

(b) NMR Analysis of the Equilibrium. The equilibrium of closed (**A**) and open (**B**) forms was investigated in CD_3OD at 296 K.^{1}H NMR spectra were recorded on a Varian Unity-300 spectrometer with ^{2}D lock. **B** form percentages were determined from the ratio of intensities of the 3′-H signals of the corresponding spirooxazines.

(c) Photokinetic Technique.[14] Absorption spectra were recorded on an Ocean Optics fiber optic diode array spectrophotometer enabling simultaneous crossed beam operation. The photochemical irradiation was derived from a 200 W high-pressure mercury lamp equipped with interference filters enabling transmissions of a selected single emission line. The monochromatic light intensity was determined directly in the reactor using either an aqueous solution of potassium ferrioxalate [I_0^{313} = (4−6 ± 0.1) 10^{-6} mol·L^{-1}·s^{-1}, I_0^{365} = (5−7 ± 0.1) 10^{-6} mol·L^{-1}·s^{-1}] or a toluene solution of Aberchrom 540 [I_0^{546} = (3−4 ± 0.1) 10^{-5} mol·L^{-1}·s^{-1}]. Then, the photon flux was checked by a semiconductor photosensor before and after each experiment. The reactor was a quartz cell (1 cm × 1 cm optical path, 2 cm^3 solution) closed with a Teflon bung. The photochromic solution was stirred continuously with a magnetic bar driven by a variable-speed stepper motor. The whole setup was enclosed in a thermostatic block (T= 283−323 K). Several wavelengths, including those for irradiation, were monitored simultaneously. The data were stored and processed on the spectrometer desk PC computer using homemade software. To determine the desired parameters, a single differential equation (eq 1) and one phenomenological one (eq 2) are used:

$$-\mathrm{d}[\mathbf{A}]/\mathrm{d}t = \mathrm{I}'_0F(\Phi_{AB}\epsilon'_A[\mathbf{A}] - \Phi_{BA}\epsilon'_B[\mathbf{B}]) - k_{AB}[\mathbf{A}] + k_{BA}[\mathbf{B}] \quad (1)$$

with

$$\mathrm{Abs} = \epsilon_A[\mathbf{A}] + \epsilon_B([\mathrm{C}]_O - [\mathbf{A}]) \quad (2)$$

$[C]_O$ is the initial concentration, $[C]_O = [\mathbf{A}] + [\mathbf{B}]$; ϵ_A and ϵ_B (l = 1 cm) are the molar absorption coefficients of the **A** and **B** forms; (′) indicates the irradiation wavelength; F is the photokinetic factor, $F = (1 - 10^{-\mathrm{Abs}'})/\mathrm{Abs}'$; and I'_0 is the incident monochromatic photon flux. Φ_{AB} and Φ_{BA} are the quantum yields of photoreactions **A** → **B** and **B** → **A**, and k_{AB} and k_{BA} are the thermal rate constants of the corresponding dark processes. In accordance with the postulated mechanism, it was shown that thermal relaxation was rigorously monoexponential for more than 97% of the kinetics, excluding any photoinduced aggregation behavior[15] or the presence of more than one kinetically coupled photoisomer. Experimental photokinetic curves (Abs_{exp}) were fitted by the model (Abs_{calc}). The values Abs_{calc} were obtained by numerical integration (Runge−Kutta semiimplicit) of eq 1 followed by application of eq 2. The residual error was $RE = \sum_p\sum_j(Abs_{calc}(j) - Abs_{exp}(j))^2/pj$, where p is the number of plots fitted simultaneously and j the number of points in each plot. The minimization algorithm is of the Powell type. Its consists of fitting parameters by returning them automatically to the numerical integration step until a minimum is reached in RE. Nine photokinetic curves were fit simultaneously (see Figure 2). Among the fifteen parameters of the model, five are known: $[C]_0$, I_0^{313}, I_0^{365}, I_0^{546} and $k_{obs} = k_{AB} + k_{BA}$, while the others (10) are adjustable: ϕ_{AB}, ϕ_{BA}, k_{AB}, ϵ_A^{313}, ϵ_A^{365}, ϵ_B^{313}, ϵ_B^{365}, ϵ_B^{546}, ϵ_B^{577}, and ϵ_B^{611}. The uniqueness of the solution was demonstrated by showing that whatever their guessed initial values, the same set was reached at convergence.

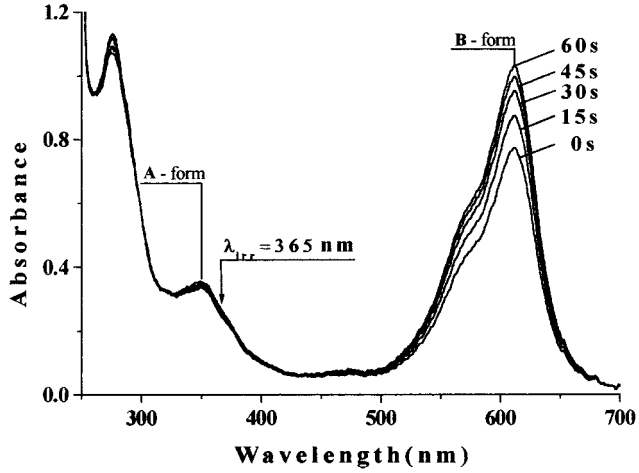

Figure 1. Absorption spectra of spirooxazine **3** in ethanol ($[C]_O = 4.5 \times 10^{-5}$ mol·L^{-1}) before and during 365 nm irradiation.

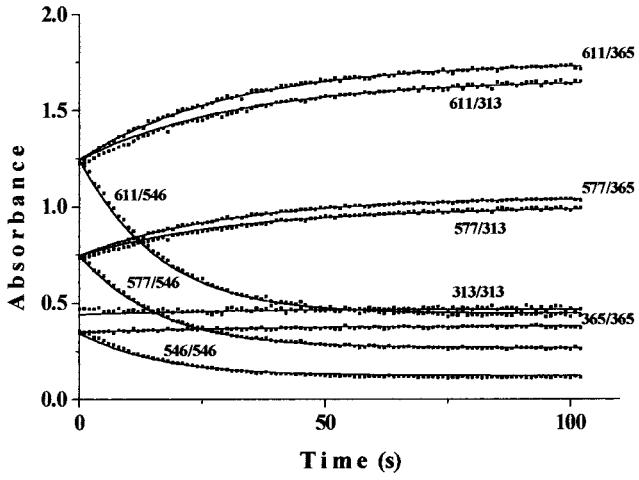

Figure 2. Absorbance of a 6.2×10^{-5} mol·L^{-1} solution of **4** in ethanol at 296 K vs time under continuous monochromatic irradiation. The first figure indicates λ_{obs}, and the second λ_{irr}. For each photokinetic run, the starting point was the thermal equilibrium position. Dots are experimental data, continuous lines are numerical fittings using the model.

Photokinetic Measurements and Data Treatment

Figure 1 shows an overlay of UV/visible spectra of **3** during irradiation.

Under UV light (where both **A** and **B** bands are irradiated), there was an increase of the open form **B** (photocoloration), while under visible irradiation (where only the **B** band was irradiated), there was a decrease of the open form (photobleaching) (shown in Figure 2). New steady states (i.e., different from the thermal equilibrium position) were reached in each case. Photoinduced variation of the absorbance under the influence of three different irradiation wavelengths (313, 365, and 546 nm) were recorded at several selected wavelengths, including the irradiation ones.

After switching off the irradiation light, the system relaxed to the initial equilibrium position. Kinetic analysis of the relaxation curves allowed the extraction of the global rate constant, $k_{obs} = k_{AB} + k_{BA}$ (Figure 3).

Photokinetic analysis of the absorbance vs time kinetic curves, as shown in Figures 2 and 3, allowed the accurate determination of the main photochromic parameters, namely, quantum yields Φ_{AB} and Φ_{BA} (assumed to be wavelength-independent), the equilibrium constant K_e, rate constants k_{AB} and k_{BA}, and molar absorption coefficients ϵ_A^{313}, ϵ_A^{365}, ϵ_B^{313}, ϵ_B^{365}, ϵ_B^{546}, ϵ_B^{577}, and ϵ_B^{611}. From the equilibrium displacements vs temperature, thermodynamic parameters $\Delta H°$ and $\Delta S°$ were also extracted. All these parameters were obtained for spirooxazines **1**−**4** in various solvents.

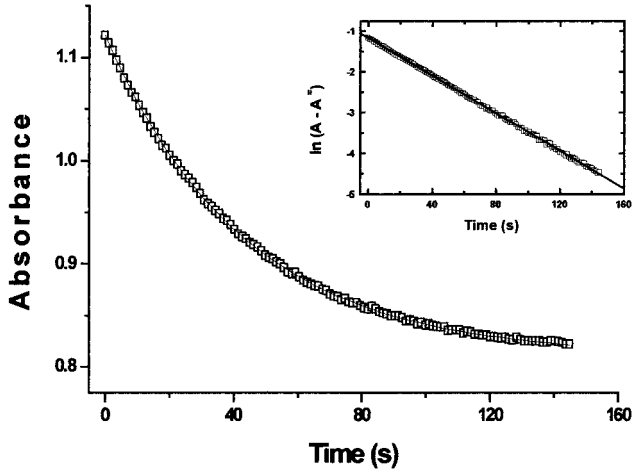

Figure 3. Thermal bleaching kinetics of **3** in ethanol at 296 K, monitored at $\lambda_{max} = 611$ nm. Inset: first-order kinetic treatment.

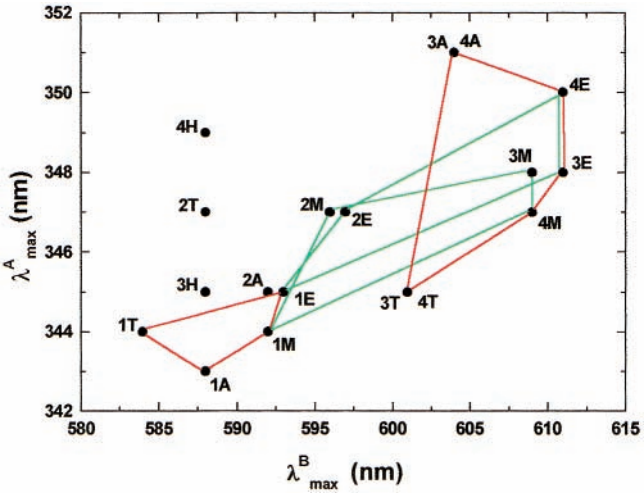

Figure 4. $\lambda-\lambda$ plots of compounds **1**−**4** in various solvents (A, acetonitrile; E, ethanol; M, methanol; T, toluene; H, *n*-heptane). Polygons have been drawn to make the figure more readable. Red polygons: illustration of the effect of *O*-alkyl substitution [**1** vs (**3** + **4**)]; Green polygons: similar behavior in ethanol and methanol (**E** vs **M**).

Results and Discussion

Spirooxazines **1**−**4** were characterized by their spectroscopic, thermodynamic, and photochromic parameters.

(a) Spectroscopic Data. The maximum absorption wavelengths of the closed (λ_{max}(**A**)) and open forms (λ_{max}(**B**)) are plotted in Figure 4 showing the relative positions of compounds **1**−**4** in various solvents. Red polygons show that, whatever the solvent, *O*-alkyl long-chain substitution in **3** and **4** induced a bathochromic effect on the absorption wavelengths of both closed and open forms (compounds **3** and **4** vs **1**). The strongest bathochromic effect was on λ_{max}(**A**) for **3** and **4** between toluene and acetonitrile, while *N*-alkyl-substituted compounds **1** and **2** appeared less solvent sensitive. On the other hand, green polygons show that whatever the compound under consideration, protic solvents ethanol (E) and methanol (M) behaved similarly; E was always close to M, while aprotic polar acetonitrile (A) and nonpolar toluene (T) behaved quite differently. These

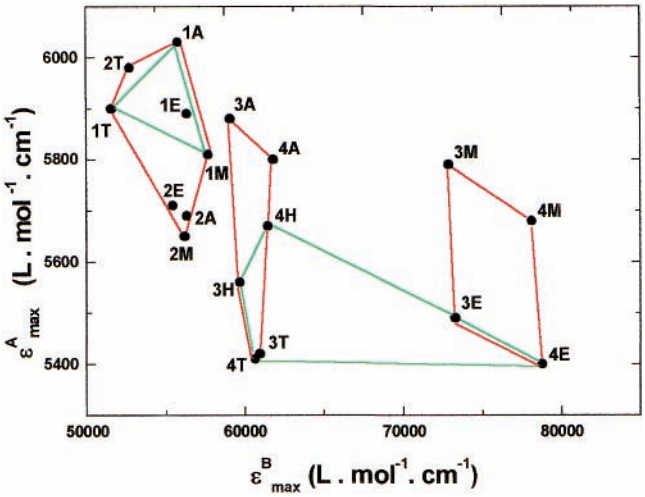

Figure 5. $\epsilon-\epsilon$ plots of compounds **1**−**4** illustrating ϵ_B and ϵ_A variations. Red polygons: ϵ_B variations according to the substituent and the solvent (**1** + **2**) vs (**3** + **4**) in nonprotic solvents vs (**3** + **4**) in alcohols). Green polygons: ϵ_A variations according to substitution [**1** vs (**3** + **4**)] in H, T, and E).

TABLE 1: Comparative Analysis of the Percentage of the Open TTC Form (B) Obtained by Two Independent Methods: NMR (CD_3OD, 296 K) and Photokinetics (CH_3OH, 296 K)

	% B			
method	**1**	**2**	**3**	**4**
NMR	11.8	24.2	31.6	31.9
photokinetics	8.1	25.4	30.2	31.2

preliminary results show that solvent and substituent effects are responsible for these spectroscopic shifts and are intimately correlated.

From $\epsilon-\epsilon$ plots (Figure 5), it appears that molar absorption coefficients are also sensitive to the solvents and the structures. Regarding the variation of ϵ_B (red polygons), it appears that several subsets can be distinguished. Compounds **1** and **2** gave the lowest ϵ_B values, whatever the solvent, while *O*-alkyl-substituted **3** and **4** were more solvent sensitive; they exhibited medium ϵ_B values in non-hydrogen bonding solvents and higher values in ethanol and methanol. For ϵ_A in toluene, *n*-heptane, and ethanol, green polygons again show the opposition between the N−CH_3-substituted **1** and the *O*-alkyl-substituted **3** and **4**.

(b) Thermodynamic Data. Equilibrium constants (K_e) were obtained by two independent methods. Table 1 shows the good correlation between NMR and photokinetic determinations.

From variable-temperature measurements, thermodynamic parameters $\Delta H°$ and $\Delta S°$ were determined. Plotting $\Delta H°$ vs $\Delta S°$ gives rise to an isothermodynamic diagram[16] (Figure 6). It shows that the thermodynamic parameters depend on the structures and the solvents. The slope of the linear fit of the diagram (not shown in the figure) corresponds to an isothermodynamic temperature of around 540 K. This rather high value indicates that under our experimental conditions (296 K), the main effect was of enthalpic origin. The higher equilibrium constants with more than 20% of **B** open form are noted as $K_e(+)$, while the lower constants with less than 10% of **B** form are noted as $K_e(-)$. In polar solvents, long-chain-substituted merocyanine compounds **2**−**4** are stabilized, while N−CH_3-substituted **1** displays a much lower equilibrium constant. This effect is seen from the red polygons. On the other hand, the green polygon shows that whatever the substitution, nonpolar solvents such as toluene and *n*-heptane only have a weak stabilization effect, giving rise to a lower equilibrium constant [$K_e(-)$].

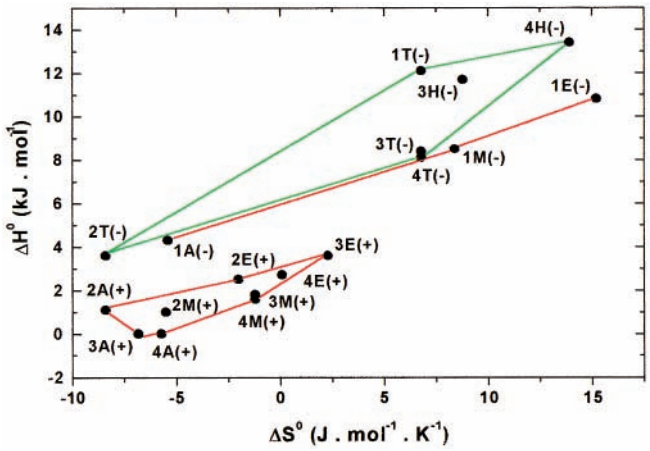

Figure 6. Isothermodynamic diagrams of spirooxazines **1**−**4** in various solvents. Red polygons: long-chain effect in polar solvents [**1** vs (**2** + **3** + **4**)]. Green polygon: low K_e for all compounds in T and H nonpolar solvents.

TABLE 2: Solvent Effect on K_e and λ_B[a]

	low K_e	high K_e
low λ_B	**1**T,A,M,E; **2**T; **3**H, **4**H neither **A** nor **B** stabilized	**2**A,M,E **B** stabilized
high λ_B	**3**T; **4**T **B*** stabilized	**3**A,M,E; **4**A,M,E **B** and **B*** stabilized

[a] **B**, open form, ground state; **B***, open form, excited state. In each case, closed form, ground state (**a**) has been taken as reference.

From the comparison of spectroscopic and thermodynamic data, it is postulated that the same solvation effects are responsible for the variations of the equilibrium position and the spectroscopic shifts. Table 2 summarizes the four main cases encountered. They were interpreted according to the stabilization of the more polar open form (**B**), taking the closed form (**A**) as a reference. When a low K_e is associated with a low λ_B (i.e., a higher energy transition), ground state (**B**) and excited state (**B***) are only weakly stabilized. This was the case for N−CH_3-substituted spirooxazine **1** in all solvents and long-chain compounds in nonpolar solvents (**2** in toluene and **3** and **4** in *n*-heptane). A high K_e with a low λ_B was interpreted as stabilization of **B** (**2** in polar solvents), while a low K_e value with a high λ_B was related to the stabilization of **B*** (**3** and **4** in toluene). The most solvatable molecules **3** and **4** in the most polar solvents (A, M, and E) are stabilized in both states **B** and **B***, giving rise to high values of both K_e and λ_B.

These results confirm that, from the solvation point of view, *O*-alkyl substitution is of more importance than N-substitution.

(c) Kinetic Data. The thermal relaxation process occurs with the apparent rate constants $k_{obs} = k_{AB} + k_{BA}$ with $k_{AB} = K_e k_{BA}$. From variable-temperature experiments, kinetic rate constants k_{AB} for **A** → **B** and k_{BA} for **B** → **A** were obtained together with the corresponding Arrhenius activation energies E_a^{AB} and E_a^{BA}. Figure 7a shows that the slowest k_{AB} and k_{BA} were exhibited by *O*-alkyl-substituted compounds **3** and **4** in alcohols, while the fastest were for **1** and **2** in acetonitrile. Except for these two extreme sets, all the remaining rate constants behaved similarly and did not exhibit any clear-cut solvent or substitution effects. It is likely that the resulting behavior was due to compensation effects.

Figure 7b is an E_a–E_a plot, it shows, as expected, that activation energies are strongly correlated with a quasilinear dependence. This effect is not surprising, as it is shown in Figure 6 that the main equilibrium effects are of enthalpic origin. For

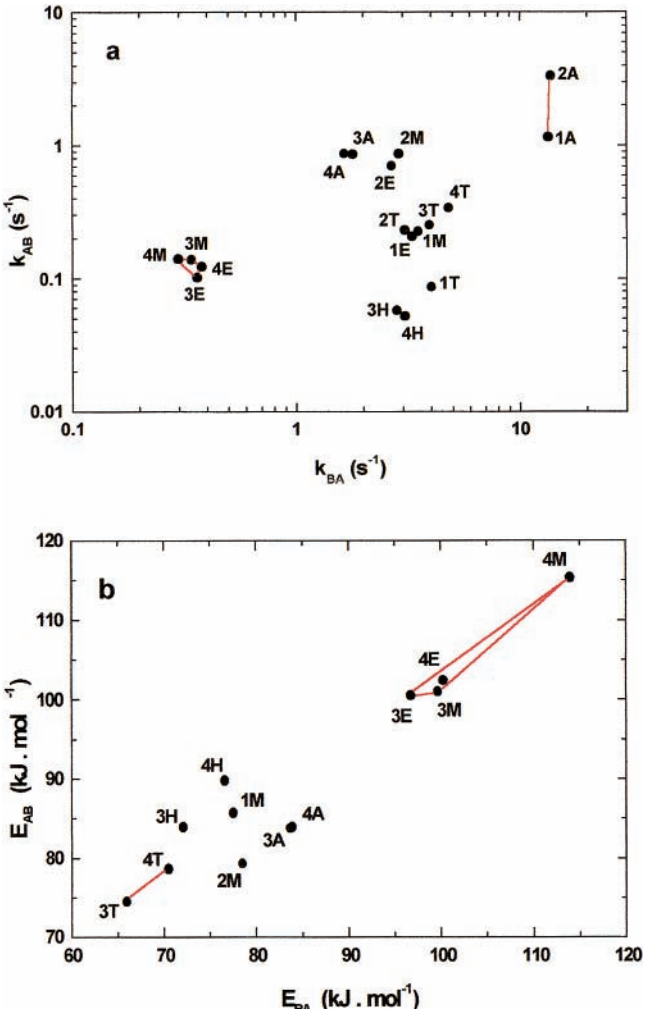

Figure 7. Structural and solvent effects on the thermal relaxation kinetics. Diagram a is a $k-k$ plot showing rate constants k_{AB} vs k_{BA}. Diagram b is an E_a-E_a plot showing activation energies. Note, in both diagrams the compensation effect for most compounds is in the medium range region.

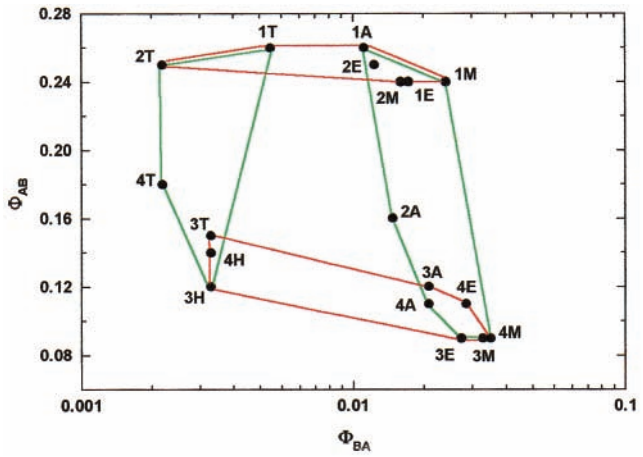

Figure 8. $\Phi-\Phi$ plot of spirooxazines **1**−**4** in various solvents. Red polygons: variation of Φ_{AB} between the *N*-alkyl- (**1** + **2**) and the *O*-alkyl-substituted (**3** + **4**) groups. Green polygons show the solvent effect on Φ_{BA} for all compounds [(T + H) vs (A + E + M)].

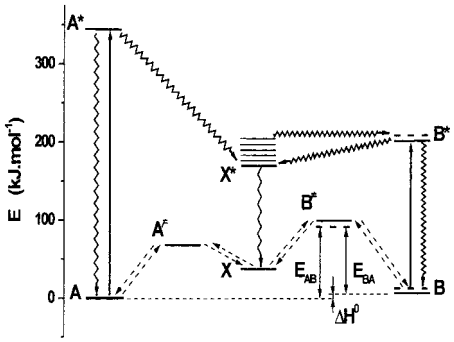

Figure 9. Schematic energy diagram for the photo- and solvatochromism of spirooxazines **1**−**4**. The closed form ground-state level (**A**) has been taken as reference. The levels of **X**, **A**‡, and **X*** are qualitative. The levels of **B**, **B**‡, **B***, and **A*** are representative of our experimental results. Solvent polarity effects are shown for **B**, **B**‡, and **B*** energy levels.

a given compound in a given solvent (S), their differences [E_a^{AB}-(S) − E_a^{BA}(S)] are of the same order of magnitude as the corresponding standard enthalpy $\Delta H°$(S). The highest activation energies are exhibited by *O*-alkyl derivatives in alcohols (**3**M, **4**M and **3**E, **4**E), in accordance with their slower kinetics. Results from thermodynamic and kinetic analysis show that **B** is higher in energy than **A** and that there is an uphill transition state in between. Moreover, for compounds **3** and **4**, it was shown that the energy level of the transition state is solvent sensitive. For instance, going from methanol (M) to toluene (T), the activation energy difference [(E_a^{AB}(M) − E_a^{AB}(T)) ≈ 26.5−36.7 kJ·mol^{-1}] is much higher than the enthalpy difference [($\Delta H°$(M) − $\Delta H°$(T)) ≈ − 6.5 to − 8.4 kJ·mol^{-1}]. This confirms that for *O*-alkyl-substituted compounds, the transition state (**B**‡) is much more solvent sensitive than the ground state (**B**).

(d) Photochemical Data. Figure 8 is a $\Phi-\Phi$ plot. Photocoloration quantum yields (Φ_{AB}) were always higher than photobleaching ones (Φ_{BA}). The ratio Φ_{AB}/Φ_{BA} ranged from 3 to 90, depending on molecular structures and solvents. A global trend is that the higher the Φ_{AB} value, the lower the Φ_{BA} value.

Except for *N*-alkyl-substituted spirooxazine **2** in acetonitrile and *O*-alkyl-substituted **4** in toluene, group (**1** + **2**) gives rise to higher Φ_{AB} values than group (**3** + **4**). Independently of the solvent, Φ_{AB}(**1** + **2**) is around 2 × Φ_{AB}(**3** + **4**). This effect is shown by red polygons. On the other hand, the green polygons show a remarkable solvent effect on Φ_{BA}: whatever the compound, Φ_{BA}(polar) is about 7 × Φ_{BA}(nonpolar). To interpret the quantum yield variations, an energy diagram including the spectroscopic, thermodynamic, and kinetic data is reported (Figure 9). Its main feature is the presence of an intermediate cisoid structure "**X**" lying between **A** and **B**. Such intermediates have been postulated from time-resolved measurement in the nanosecond[17] to the picosecond[18] and femtosecond[19] domain and, in the particular case of spiropyrans, from semiempirical calculations.[20] The kinetic behavior of **X** is decisive for the relative values of the quantum yields Φ_{AB} and Φ_{BA}. The successive processes **X*** → **X** → α**A** + (1 − α)**B**[21] show that the simple variation of the branching ratio α is likely to give rise to a global negative correlation between Φ_{AB} and Φ_{BA}. For compounds **3** and **4**, the highest activation energies correspond to the highest Φ_{BA} (in M and E) and that the lowest E_a are related to the lowest Φ_{BA} (in T), the solvent effect on Φ_{BA} can be interpreted by a higher **B**‡ transition state in polar solvents. Figure 9 shows that a higher **B**‡ transition state is related to a higher branching ratio α and consequently to a higher Φ_{BA}. A high E_a is associated with a high Φ_{BA} and a low Φ_{AB}, while a lower E_a is related to a lower Φ_{BA} and a higher Φ_{AB}. Solvent rearrangement due to polarity changes and volume increase at the onset of ring closure is the most probable origin of the energy increase in the transition state **B**‡. This assumption is supported by pretty good linear correlations (R > 0.994) between the

acceptor numbers (AN)[22] of the solvents and Φ_{BA}: the higher AN, the higher Φ_{BA}. These correlations show that **3** and **4** behave very similarly and are the most solvent sensitive, while **1** and **2** are less so.

Other isomerization paths are also to be considered. For instance, some increase of Φ_{AB} with temperature is likely to originate from the direct population of **B*** from the highest vibrational levels of **X***. The possible solvent-induced deactivation of the excited states can also be taken into account to interpret the quantum yield variations more accurately.

Conclusion

For the first time, the quantum yields of the photoinduced **A** → **B** and **B** → **A** processes, the rate constants of the thermal rearrangements, and the equilibrium position of a series of four semipermanent merocyanines have been determined in different solvents and at various temperatures using photokinetic analysis of absorbance vs time curves recorded under continuous monochromatic irradiation. The values of the equilibrium constants extracted from the photokinetics fit well with those obtained from entirely independent NMR measurements.

O-Alkyl-substituted merocyanines **3** and **4** exhibit a subtle solvation behavior. They are weakly solvated in the less polar solvent *n*-heptane. They are solvated in toluene but only in the excited state and solvated both in ground and excited states in acetonitrile and alcohols. *N*-Alkyl-substituted merocyanine **2** behaves quite differently; its ground state is more solvated in the polar solvents, but less so in toluene. N−CH_3-substituted **1** appears to be less solvent sensitive. For all compounds in all solvents, the photocoloration quantum yield Φ_{AB} was higher than the photobleaching yield Φ_{BA}. The highest Φ_{AB} values were for *N*-alkyl compounds **1** and **2**. Moreover, Φ_{BA} was solvent sensitive. Whatever the substituents, the lowest Φ_{BA} values were in nonpolar solvents, while the highest were in polar media. An energy diagram including the presence of an excited (**X***) and a ground state (**X**) short-lived cisoid intermediate was established. It allows us to interpret the whole set of solvent effects on spectroscopic data, equilibrium position, rate constants, activation energies, and quantum yields. The relative solvation of the semipermanent merocyanine in the ground and transition states depends on the polarity and proticity of the solvent and on the substitution of the spirooxazine.

Acknowledgment. One of us (A.V.M) gratefully acknowledges a RFBR endowment (99 03 32485) and a grant from the Program International de Coopération Scientifique (PICS 705) between the Centre National de la Recherche Scientifique C.N.R.S. (France) and the Russian Academy of Sciences (R.A.S.).

References and Notes

(1) (a) Rouvray, D. *Chem. Br.* **1998**, *34*, 26. (b) Feringa, B. L.; Huck, N. P. M.; Shoevaars, A. M. *Adv. Mater.* **1996**, *8*, 681. (c) Malkin, J.; Zelichenok, A.; Krongauz, V.; Dvorkinov, A. S.; Rentzepis, P. M. *J. Am. Chem. Soc.* **1994**, *116*, 1101. (d) Irie, M.; Uchida, K.; *Bull. Chem. Soc. Jpn.* **1998**, *71*, 985.

(2) Chu, N. Y. C. In *Photochromism, Molecules and Systems*; Dürr, H., Bouas-Laurent, H., Eds.; Elsevier: 1990; Chapter 10, p 493; ISBN: 0-444-87432-1.

(3) Malatesta, V.; Ranghino, G.; Romano, U.; Allegrini, P. *Int. J. Quantum Chem.* **1992**, *42*, 879.

(4) Nakamura, S.; Uchida, K.; Murakami, A.; Irie, M. *J. Org. Chem.* **1993**, *58*, 5543.

(5) Micheau, J. C.; Lavabre, D. *EPA Newslett.* **1986**, *March*, 26.

(6) Rau, H.; Greiner, G. *EPA Newslett.* **1991**, *March*, 40.

(7) (a) Pimienta, V.; Levy, G.; Lavabre, D.; Samat, A.; Guglielmetti, R.; Micheau, J. C. *Mol. Cryst. Liq. Cryst.* **1994**, *246*, 2839. (b) Favaro, G.; Malatesta, V.; Mazucatto, U.; Ottavi, G.; Romani. A. *J. Photochem. Photobiol. A: Chem.* **1995**, *87*, 235. (c) Deniel, M. H.; Tixier, J.; Lavabre, D.; Micheau, J. C.; Dürr, H. *Mol. Cryst. Liq. Cryst.* **1997**, *298*, 129. (d) Zhou, J.; Li, Y.; Tang, Y.; Zhao, F.; Song, X. *Acta Phys. Chim. Sinica.* **1995**, *11* (2), 97.

(8) (a) Chu, N. Y. C. *Can. J. Chem.* **1983**, *61*, 300. (b) Samat, A.; Loshkin, V. in *Organic Photochromic and Thermochromic Compouds*; Crano, J. C., Guglielmetti, R. J., Eds.; Plenum Press: New York, 1999; Vol. 2, p 415. (b) Nishimura, N.; Miyake, J.; Sueishi, Y. *Bull. Chem. Soc. Jpn.* **1989**, *62*, 1777.

(9) Rau, H.; Greiner, G.; Gauglitz, G.; Meir, H. *J. Phys. Chem.* **1990**, *94*, 6523.

(10) (a) Favaro, G.; Masetti, F.; Mazucatto, U.; Ottavi, G.; Allegrini, P.; Malatesta, V. *J. Chem. Soc., Faraday Trans* **1994**, *90* (2), 333. (b) Favaro, G.; Malatesta, V.; Mazzucato, U.; Miliani, C.; Ottavi, G. *Proc. Indian Acad. Sci.(Chem. Sci.)* **1995**, *107* (6), 659.

(11) Gauglitz, G.; Stössel, P.; Meier, H.; Rau, H. *J. Photochem. Photobiol. A: Chem.* **1995**, *85*, 207.

(12) (a) Wilkinson, F.; Hobley, J.; Naphthaly, M. *J. Chem. Soc., Faraday Trans* **1992**, *88* (11), 1511. (b) Pimienta, V.; Lavabre, D.; Levy, G.; Samat, A.; Guglielmetti, R.; Micheau, J. C. *J. Phys. Chem. 100* (10) 4485. (c) Deniel, M. H.; Tixier, J.; Houzé-Luccioni, B.; Lavabre, D.; Micheau, J. C. *Mol. Cryst. Liq. Cryst.* **1997**, *298*, 121.

(13) (a) Khairutdinov, R. F.; Giertz, K.; Hurst, J. K.; Voloshina, E. N.; Voloshin, N. A.; Minkin, V. I. *J. Am. Chem. Soc.* **1998**, *120*, 12708. (b) Pozzo, J. L.; Samat, A.; Guglielmetti, R.; de Keukeleire, D. *J. Chem. Soc., Perkin Trans 2*, **1993**, *2*, 1327.

(14) Deniel, M. H.; Lavabre, D.; Micheau, J. C. In *Organic Photochromic and Thermochromic Compounds*; Crano, J. C., Guglielmetti, R. J., Eds.; Plenum Press: New York, 1999; Vol. 2, p 167.

(15) Li, Y.; Zhou, J.; Wang, Y.; Zhang, F.; Song, X. *J. Photochem. Photobiol. A: Chem.* **1998**, *113*, 65.

(16) Schmid, R.; Sapunov, V. *Non Formal Kinetics, Monograph in Modern Chemistry*, 14; Verlag Chemie: 1982; ISBN: 0-89573-055-3.

(17) (a) Bohne, C.; Fan, M. G.; Li, Z. J.; Lusztyk, J.; Scaiano, J. C. *J. Chem. Soc. Chem. Commun.* **1990**, 571. (b) Bohne, C.; Fan, M. G.; Li, Z. J.; Liang, Y. C.; Lusztyk, J.; Scaiano, J. C. *J. Photochem. Photobiol. A: Chem.* **1992**, *66*, 79.

(18) (a) Aramaki, S.; Atkinson, G. H. *Chem. Phys. Lett.* **1990**, *170* (2−3), 181. (b) Wilkinson, F.; Worrall, D. R.; Hobley, J.; Jansen, L.; Williams, S. L.; Langley, A. J.; Matousek, P. *J. Chem. Soc., Faraday Trans* **1996**, *92* (8), 1331.

(19) (a) Tamai, N.; Masuhara, H. *Chem. Phys. Lett.* **1992**, *191* (1,2), 189. (b) Schneider, S.; Mindl, A.; Elfinger, G.; Melzig, M. *Ber. Bunsen-Ges. Phys. Chem.* **1987**, *91*, 1222.

(20) Wojtyck, J. T. C.; Wasey, A.; Kazmeir, P. M.; Hoz, S.; Buncel, E. *J. Phys. Chem. A* **2000**, *104*, 9046.

(21) Chibisov, A. K.; Görner, H. *J. Phys. Chem. A* **1997**, *101*, 4305.

(22) See ref 16, p 141.